

# Unified framework for finding eigenstates of Helmholtz equation using boundary methods

Doron Cohen<sup>1,2</sup>, Natasha Lepore<sup>2</sup> and Eric J. Heller<sup>2,3</sup>

<sup>1</sup> *Department of Physics, Ben-Gurion University, Beer-Sheva, Israel.*

<sup>2</sup> *Department of Physics, Harvard University, Cambridge, Massachusetts.*

<sup>3</sup> *Department of Chemistry and Chemical Biology, Harvard University, Cambridge, Massachusetts.*

(Dated: June 2001)

The powerful plane-wave decomposition method (PWDM) for finding eigenstates of Helmholtz equation can be regarded as a variant of the mathematically well-established boundary integral method (BIM). The capabilities of the BIM and the PWDM are discussed using a unified framework. This opens the way to further improvements.

## I. INTRODUCTION

Solving Helmholtz equation within a domain, given Dirichlet boundary conditions, is of great interest in Physics [1], and has important engineering applications. Helmholtz equation is the simplest example for a *wave equation*. This equation can describe acoustics waves, microwave systems, and in particular it describes the wavefunction of a quantal particle inside a cavity. It has become a prototype problem in studies of ‘quantum chaos’, and it has applications in studies of nano-scale mesoscopic devices [2], such as quantum-dots, where the motion of the electrons can be regarded as a free motion within a ‘box’. Of particular interest are the wavefunctions of a stationary particle in a two-dimensional box (so called ‘billiard system’). Solutions of Helmholtz equation have been shown to exhibit the scarring phenomena [3]. Some related properties of the solutions are important for studies of quantum transport.

The wavefunction  $\Psi(x)$  of a stationary particle in a two-dimensional (2D) box (so called ‘billiard system’) is a solution of the homogeneous Helmholtz equation  $\mathcal{H}\Psi(x) = 0$ . The differential operator  $\mathcal{H}$  is defined as

$$\mathcal{H} = -\nabla^2 - k^2. \quad (1)$$

Note that for the special case  $k = 0$ , the Helmholtz equation reduces to Laplace’s equation. Given a closed boundary we can ask whether this equation has a non-trivial solution that satisfies Dirichlet boundary conditions  $\Psi(x) = 0$ . The values  $k = k_n$  for which there are non-trivial solutions are the eigenvalues, and the corresponding  $\Psi(x)$  are the eigenfunctions.

Two main numerical strategies have been suggested to date in the literature in order to find the eigenstates of Helmholtz equation. The first strategy can be described as a ‘Laplacian diagonalization’. A basis is selected such that the functions it contains satisfy the Dirichlet boundary conditions. For example, in some cases one can use conformal mapping to determine a basis [4] (and see also [5]). After a basis is selected, the Laplacian operator is written in this basis and then diagonalized. In practice, some truncation is required. Consequently the diagonalization determines all the eigenstates up to some

maximum wavenumber  $k_{\max}$ . Thus, the Laplacian diagonalization strategy is inherently limited, and can not be used for the purpose of finding high-lying eigenstates.

The second numerical strategy, which is the object of this paper, can be described as a ‘boundary approach’. This strategy is based on the observation that the eigenfunctions are completely determined by their behavior at the boundary. For 2D billiards the ‘Laplacian diagonalization’ requires 2D grid calculations. This is a heavy numerical task. The ‘boundary approach’ on the other hand reduces the calculations to a 1D boundary grid. As we are going to explain, the search of eigenstates can be restricted to a small  $k$  window that contains the energy range of interest. Therefore the method is naturally suitable for the purpose of finding high-lying eigenstates.

In the ‘quantum chaos’ community, two boundary methods are commonly employed. The first one is referred to as the boundary integral method (BIM) [6], while the other is the decomposition method (DEM). The plane-wave decomposition method (PWDM) [7] can be viewed as a special case of the DEM. Related versions of PWDM have been used in [8, 9] and in [10].

Usually, the BIM and the PWDM are considered to be two independent and self-contained procedures, and several studies have been done in order to compare them [11]. In the present paper, we adopt a different point of view. We regard the BIM and the DEM as a sequence of four independent steps. By doing so, we are going to make the observation that the DEM and the BIM are strongly related. In order to bridge between them, we will highlight an intermediate strategy which we call the gauge-freedom method (GFM). Finally, the general framework that we set opens the way for further improvements [12].

The numerical procedure for finding the eigenvalues and the eigenfunctions can be summarized by a set of four steps that is common to the BIM and the DEM, and as we will show later, to the GFM:

- Choice of a set of basis functions  $F_j(x; k)$ .
- Definition of the Fredholm matrix  $\mathbf{A}_{js}(k)$ .
- Procedure for construction of the wavefunction  $\Psi_\tau$ .

- Definition of the quantization measure  $S(k)$ .

The first step consists of selecting a set of basis functions  $F_j(x; k)$  labeled  $j = 1..N$ . All boundary methods rely on basis functions that satisfy the Helmholtz equation *inside* the billiard. Thus, a superposition of such basis functions is an eigenfunction if it vanishes along the boundary. The choices of bases that correspond to the PWDM, to the primitive version of the BIM and to the simplest variation of the GFM are as follows:

$$F_j(x; k) = \cos(\phi_j + kn_j \cdot x) \quad \text{PWDM} \quad (2)$$

$$F_j(x; k) = Y_0(k|x - x_j|) \quad \text{Y0-BIM} \quad (3)$$

$$F_j(x; k) = J_0(k|x - x_j|) \quad \text{J0-GFM} \quad (4)$$

For the purpose of the numerical treatment we represent the boundary by a set of points  $x_s$  with  $s = 1 \dots M$ . In practice, we choose a set of  $M$  equally spaced points, so that the spacing is  $\Delta s = L/M$  where  $L$  is the perimeter of the billiard. Depending on details of the numerical strategy, the number of points along the boundary is either taken to be equal to the number of basis functions ( $M = N$ ), or it may be larger ( $M > N$ ). The Fredholm matrix is defined as

$$\mathbf{A}_{js}(k) \equiv F_j(x_s; k) \quad (5)$$

Given  $k$ , one may perform the singular value decomposition (SVD) of the matrix  $\mathbf{A}$ . The normalized right-vector that correspond to the smallest singular value will be denoted by  $\Phi_s$ , while the corresponding left-vector will be denoted by  $\mathbf{C}_j$ . The smallest singular value is  $\|\mathbf{A}\Phi\| = \|\mathbf{C}\mathbf{A}\|$ .

In the third step, the eigenvectors  $\Phi_s$  and  $\mathbf{C}_j$  are used to construct a wavefunction  $\Psi_r$  through a linear transformation. We select a grid of points  $X_r$  on which the wavefunction  $\Psi_r \equiv \Psi(X_r)$  is calculated. In the traditional DEM, the left eigenvector  $\mathbf{C}$  is used for the purpose of this construction, and the linear transformation which is applied is:

$$\Psi_r = \sum_j \mathbf{C}_j \mathbf{F}_{jr} \quad (6)$$

where  $\mathbf{F}_{jr} \equiv F_j(X_r; k)$ . Note that  $\mathbf{C}$  contains the expansion coefficients of  $\Psi(x)$  in the chosen basis  $F_j(x; k)$ . For the BIM, the right eigenvector  $\Phi$  is traditionally used in order to build the wavefunction, and the linear transformation in this case is

$$\Psi_r = \sum_s \mathbf{G}_{rs} \Phi_s, \quad (7)$$

where  $\mathbf{G}_{rs}$  is the discretized version of the Green function. Thus, the vector  $\Phi_s$  represents a ‘charge’ that is distributed along the boundary. For completeness, we explain this point in the next section.

In the final step, a measure  $S(k)$  is defined such that  $S(k) = 0$  if  $k$  is an eigenvalue and  $S(k) > 0$  otherwise. In practice, the eigenvalues are determined by searching for

the local minima of  $S(k)$ . By construction, the wavefunction which was built in step three satisfies the Helmholtz equation inside the boundary. Therefore, the most natural choice of  $S(k)$  is the ‘tension’, which is a measure for the roughness of the constructed  $\Psi(x)$  along the boundary. This definition of  $S(k)$  is traditionally used with the PWDM. Other known possibilities for the measure include the smallest singular value, and the Fredholm determinant of  $\mathbf{A}$ . These two latter choices of  $S(k)$  are the ones that are usually associated with the BIM. In Sec. V we discuss the mathematical equivalence of the three possible measures, and compare their respective numerical effectiveness.

The structure of this paper is as follows: In Sec. II, we give a concise presentation of the BIM and the related GFM. Strategies for the construction of the wavefunction are discussed in Sec. III. Sec. IV explains how the GFM bridges between the BIM and the DEM. Sec. V contains a description of the possible choices for the quantization measure, as well as a comparison between the numerical accuracies of the BIM and the PWDM.

The shape that we have studied numerically is presented in Fig.1. We have used the cornerless, generic ‘Pond’ shape in order to avoid a range of problems that arise with more complicated geometries. These problems are the subject of a follow-up study [12], where we suggest effective (mixed BIM/DEM) methods for finding eigenfunctions. This is done using the above theoretical framework, while regarding the ‘Pond’ shape as a reference against which to judge the effectiveness of our efforts. For the convenience of the reader, our numerical notations are concentrated in Table 1. Further information about Fig.1, Table 1, and the numerical analysis is integrated within the main text.

## II. THE BIM AND THE GFM

The free space Green function  $G(x, x')$  is defined by the equation  $\mathcal{H}G(x, x') = \delta(x - x')$ . The most general solution can be written as

$$G(x, x') = -\frac{1}{4}Y_0(k|x - x'|) + \mathcal{C}(x, x') \quad (8)$$

where  $\mathcal{C}(x, x')$  is any solution of the homogeneous equation  $\mathcal{H}\mathcal{C}(x, x') = 0$ . Note that in the electrostatic limit  $k \rightarrow 0$  we have  $G(x, x') = -(1/(2\pi)) \ln(r) + \mathcal{C}$ , where  $\mathcal{C}$  is a constant. We shall refer to the choice of  $\mathcal{C}(x, x')$  as gauge freedom.

By the definition of the Green function, it follows that a solution of the generalized Poisson-Laplace (GPL) equation  $\mathcal{H}\Psi(x) = \rho(x)$  is

$$\Psi(x) = \int G(x, x')\rho(x')dx' \quad (9)$$

We refer to  $\rho(x)$  as the ‘charge density’, by analogy to its electrostatic equivalent. We shall use the notation  $\Phi(s)$

$x_s$	=	vector of boundary points
$x_s$	=	vector of outer-boundary points
$X_r$	=	vector of interior grid points
$X_0$	=	a selected interior point
$\Psi_r$	=	wavefunction on the grid points
$\Psi_s$	=	wavefunction on the boundary points
$\Phi_s$	=	'charge' along the boundary
$\ \Psi_r\ $	=	norm of the wavefunction (see Sec.III)
$\ \Psi_s\ $	=	tension of the wavefunction (see Sec.III)
$n(s)$	=	unit normal at the boundary point $x_s$
$\mathbf{w}_s$	=	$(1/(2k^2)) n(s) \cdot x_s$
$\mathbf{G}_{rs}$	=	$G(X_r, x_s)$
$\mathbf{A}_{j0}$	=	$F_j(X_0; k)$
$\mathbf{A}_{js}$	=	$F_j(x_s; k)$
$\mathbf{D}_{js}$	=	$\partial F_j(x_s; k)$
$\mathbf{B}_{ij}$	=	$\Delta s \sum_s \mathbf{w}_s \mathbf{D}_{is} \mathbf{D}_{js} = \Delta s (\mathbf{D} \mathbf{w} \mathbf{D}^\dagger)_{ij}$
$\mathbf{T}_{ij}$	=	$\Delta s \sum_s \mathbf{A}_{is} \mathbf{A}_{js} = \Delta s (\mathbf{A} \mathbf{A}^\dagger)_{ij}$

TABLE I: Notations

in order to refer to (surface) charge density upon the boundary. In the latter case, the equation above reduces to

$$\Psi(x) = \oint G(x, x(s)) \Phi(s) ds \quad (10)$$

where  $s$  parameterizes the boundary. For numerical purposes, it is convenient to use the discretized version Eq.(7) of the above formula: the Green function matrix is  $\mathbf{G}_{rs} = G(X_r, x_s)$ , and the boundary charge vector is  $\Phi_s = \Phi(s) \Delta s$ , where  $\Delta s$  is the spacing between the boundary points.

### A. The BIM

Let us assume that  $k$  is an eigenvalue of the Helmholtz equation with Dirichlet boundary conditions. In such a case, we have a non-vanishing  $\Psi(x)$  inside the boundary that satisfies  $\Psi(x) = 0$  on the boundary. It follows from Green's theorem that the interior wavefunction satisfies Eq.(10) with

$$\Phi(s) = \partial_- \Psi(x(s)) \equiv \lim_{x \uparrow x(s)} n(s) \cdot \nabla \Psi(x) \quad (11)$$

The unit vector  $n(s)$  at the boundary point  $s$  is a normal to the boundary and points outwards. The notation  $\partial_-$

is used for the normal derivative evaluated inside of the billiard walls.

The BIM is based on the above observation, which we would like to paraphrase as follows: If an eigenstate  $\Psi(x)$  exists, then there also exists (by Eq.(11)) a charge density  $\Phi(s)$  such that Eq.(10) is satisfied. In particular, on the boundary we have

$$\int G(x(j), x(s)) \Phi(s) ds = 0 \quad [\text{BIM equation}] \quad (12)$$

In other words, having an eigenstate  $\Psi(x)$  implies that the kernel  $G(x(j), x(s))$  has an eigenvector that corresponds to a zero eigenvalue. The converse is also true: If we can find a non-trivial  $\Phi(s)$  that satisfies Eq.(12), then, using Eq.(10), we can construct a solution for Helmholtz equation that satisfies Dirichlet boundary conditions. We discuss this construction issue in more details in the next section. Fig.2 shows an example of a boundary charge density  $\Phi(s)$  that was found via the BIM equation (for more details, see next section).

For numerical purposes, the BIM equation can be written as the matrix equation  $\mathbf{A} \Phi = 0$ , where  $\mathbf{A}_{js} = G(x(j), x(s))$ . Using the Neumann Bessel function  $Y_0(k|x-x'|)$  for the Green function, one obtains the matrix  $\mathbf{A}_{js}$  as defined by Eq.(5) with (3). Another possibility is to use the Hankel Bessel function  $H_0(k|x-x'|)$ . Accordingly, we will distinguish between the Y0-BIM version and the H0-BIM version. We shall later discuss the numerical implication of using the complex  $H(k|x-x'|)$  rather than the real  $Y(k|x-x'|)$ .

The primitive BIM uses Eq.(12) literally. It can be easily generalized to handle scattering problems (Appendix A). However, the primitive BIM version is not the one that is generally favored because  $G(x(j), x(s))$  is singular for  $x(j) \rightarrow x(s)$ , leading to some difficulty in determining the diagonal matrix elements of  $\mathbf{A}_{js}$ . Therefore, another version of the BIM has become popular (see Appendix B). This latter version involves either the  $Y_1(k|x-x'|)$  or the  $H_1(k|x-x'|)$  Bessel function. Accordingly, we shall refer to it as either the Y1-BIM or the H1-BIM, respectively.

### B. The GFM

The GFM is a different strategy to obtain the charge density  $\Phi(s)$ . Rather than using the BIM equation Eq. (12) or one of its variants, a gauge freedom argument is invoked in order to introduce a new type of equation (Eq.(13) below). It is clear that Eq.(12) should be valid for *any* choice of gauge. In other words, Eq.(12) should be satisfied with any Green function (Eq.(8)), whatever is the choice of  $\mathcal{C}(x, x')$ . Therefore, for a given  $\mathcal{C}(x, x')$ , the charge density  $\Phi(s)$  must satisfy the equation

$$\int \mathcal{C}(x(j), x(s)) \Phi(s) ds = 0 \quad [\text{GFM equation}] \quad (13)$$

For example, we may take  $\mathcal{C}(x, x') = J_0(k|x - x'|)$ . In such a case, the GFM equation can be written as the matrix equation  $\mathbf{A}\Phi = 0$ , corresponding to the choice of Eq.(4). We shall refer to this version of GFM as J0-GFM.

The kernel  $\mathbf{A}_{js} = J_0(k|x - x'|)$  of the J0-GFM is non-singular, and very well-behaved. Thus, the J0-GFM method, unlike the Y0-BIM, provides an extremely convenient way to obtain the eigenvalues of the Helmholtz equation. Fig.2 shows an example of a charge density that was found via the J0-GFM equation (for more details see next section). The result is indistinguishable from the  $\Phi(s)$  that is generated by the traditional H1-BIM. [We note however that the J0-GFM method has certain numerical limitations that we are going to discuss later]. Once the eigenvector  $\Phi(s)$  is found via the GFM equation, we can proceed as with the traditional BIM, and construct the wavefunction  $\Psi(x)$  using Eq.(7).

### III. CONSTRUCTING THE WAVEFUNCTION

#### A. Green function method (Eq. (7))

Both the BIM equation (Eq.(12)) and the GFM equation (Eq.(13)) can be written as the matrix equation  $\mathbf{A}\Phi = 0$  for the charge vector  $\Phi_s$ . The only difference between the two is in the choice of  $\mathbf{A}$ . The numerical procedure for solving the BIM/GFM equation is as follows: Given  $k$ , one performs the SVD of the matrix  $\mathbf{A}$ . Fig.4 displays an example of the output of such a SVD procedure. One then finds the right eigenvector  $\Phi$  that corresponds to the *smallest* singular value. Whenever the smallest singular value equals zero (in a numerical sense), the  $\Phi$  constitutes a non-trivial solution of the BIM/GFM equation, and the corresponding  $k = k_n$  is an eigenvalue of the Helmholtz equation.

Once the charge vector  $\Phi_s$  has been determined, as in the example of Fig.2, one can construct the wavefunction using Eq.(7). For the Green function (Eq.(8) it is most natural to use the simplest gauge ( $\mathcal{C} = 0$ ). Any different gauge should give the same result, and in particular any complex part should vanish anyway. The outcome of the Green function method is illustrated in Fig.3. In the following paragraphs we are going to discuss the practical issue of wavefunction normalization, and then to explain why the constructed wavefunction vanishes outside of the boundary.

In a practical numerical implementation, the vector  $\Phi_s$  is normalized in the sense  $\sum_s |\Phi_s|^2 = 1$ , and therefore  $\Psi_r$  does not have proper normalization within the interior region. Adopting the usual philosophy of boundary methods, the problem of calculating the  $\Psi_r$  normalization is reduced to that of evaluating a boundary integral, namely [6, 13]

$$\int |\Psi(x)|^2 dx = \frac{1}{2k^2} \oint |\Phi(s)|^2 (n(s) \cdot x(s)) ds \quad (14)$$

By discretizing Eq. (14), we obtain the following numerical expression for the proper normalization factor:

$$\|\Psi_r\| = \frac{1}{\Delta s} \sum_s \mathbf{w}_s (\Phi_s)^2 = \Phi^\dagger \mathbf{W} \Phi \quad (15)$$

where  $\mathbf{W} = (1/\Delta s)\text{diag}(\mathbf{w}_s)$  is a diagonal matrix, and the weight factor  $\mathbf{w}_s$  is defined in Table 1.

Once we have settled the question of the wavefunction inside the boundary, it is natural to ask what is  $\Psi(x)$  outside of it. The answer turns out to be  $\Psi(x) = 0$ . For completeness, we give a proof of this statement. Let us define an extended function  $\Psi_{\text{ex}}(x)$  such that  $\Psi_{\text{ex}}(x) = \Psi(x)$  inside and  $\Psi_{\text{ex}}(x) = 0$  outside of the boundary. We would like to show that  $\Psi(x)$  as defined by Eq.(10) is also equal to  $\Psi_{\text{ex}}(x)$  outside of the boundary. It is clear that  $\Psi(x)$  is a solution of the GPL equation by construction [see discussion following Eq.(9)]. In the next paragraph, we are going to argue that  $\Psi_{\text{ex}}(x)$  is a solution of the *same* GPL equation. It follows that the difference  $R(x) = \Psi(x) - \Psi_{\text{ex}}(x)$  is a solution of Helmholtz equation in free space. From the definition of  $\Psi_{\text{ex}}(x)$ , we have  $R(x) = 0$  in the interior region, which implies by the unique continuation property that  $R(x) = 0$  over all space.

The proof that  $\Psi_{\text{ex}}(x)$  is a solution of the GPL equation with a charge density given by Eq.(11) goes as follows: By construction,  $\Psi_{\text{ex}}(x)$  satisfies the GPL equation inside as well as outside of the boundary. All we have to show is that it also satisfies the GPL equation across the boundary. The latter statement is most easily established by invoking Gauss' law. This approach is valid because at short distances,  $G(x, x')$  coincides with the electrostatic Green function. Thus, the gradient of  $\Psi_{\text{ex}}(x)$  corresponds, up to a sign, to the electric field. Gauss' law implies that the electric field should have a discontinuity equal to the charge density  $\Phi(s)$ . Indeed,  $\Psi_{\text{ex}}(x)$  is consistent with this requirement.

The numerical wavefunction  $\Psi_r$  satisfies Helmholtz equation in the interior region *by construction*. Thus, whether  $\Psi_r$  is an actual eigenstate depends on its behavior near the boundary. Following [7] we would like to define a 'tension' measure in order to estimate whether, and to what accuracy, the numerical  $\Psi_r$  satisfies the boundary conditions. In the context of the PWDM, the tension is defined as the integral of  $|\Psi(x)|^2$  along the boundary. For the BIM on the other hand, this definition is not practical due to the singular nature of the basis functions. For any finite  $M$ , the numerical wavefunction blows up at each boundary point. However, since the BIM wavefunction vanishes everywhere outside of the billiard, a numerically unambiguous definition of tension arises as an integral of  $|\Psi(x)|^2$  along an outer-boundary:

$$\|\Psi_s\| = \Delta s \sum_s (\Psi_s)^2 = \Delta s \sum_s \left( \sum_s \mathbf{G}_{ss} \Phi_s \right)^2 \quad (16)$$

By 'outer boundary' (see Fig.1), we mean the set of external points ( $s$  points, as opposed to  $s$  points for the

true boundary) that have a fixed transverse distance  $\Delta L$  from the true boundary. The distance  $\Delta L$  between the boundary and the outer-boundary should be small on any classical scale but large compared with  $ds$ , in order for the tension to be independent of the choice of  $\Delta L$ . See Fig.5c for a numerical demonstration.

### B. Decomposition method (Eq. (6))

The other procedure to construct the wavefunction is to use Eq.(6). The idea is to regard  $F_j(x; k)$  as a basis for the expansion:

$$\Psi(x) \approx \sum_j C_j F_j(x; k) \quad (17)$$

The PWDM is a special case of the DEM, corresponding to the choice Eq.(2) of basis functions. Any such superposition is a solution of Helmholtz equation within the interior region. Naively, in order to satisfy the Dirichlet boundary conditions, we should look for a vector  $\mathbf{C}$  of expansion coefficients that satisfy  $\mathbf{C}\mathbf{A} = 0$ . However, the actual implementation of this idea is associated with a numerical problem which we are going to explain below. In later subsections, we discuss the actual methods for the determination of  $\mathbf{C}$ .

In Fig.2, we display an example of a numerically determined  $\mathbf{C}$  for one of the Pond eigenstates, while in Fig.3 we illustrate the constructed wavefunction. Unlike the Green function construction, the DEM/PWDM constructed wavefunction does not vanish outside of the boundary. Actually, it is quite the opposite: Typically the DEM/PWDM wavefunction becomes exponentially large as we go further outside. Whenever this happens, it constitutes an indication for the *evanescent* nature of the wavefunction. Namely, in typical cases, in order to accommodate itself to the boundary, the wavefunction should contain sub-wavelength features. This requires exponential behavior (negative kinetic energy) in the transverse space direction.

One may think that a practical numerical definition for  $\mathbf{C}$  would be as the (left) eigenvector that corresponds to the smallest singular value of  $\mathbf{A}_{js}$ . However, in a practical numerical procedure, this definition is hard to implement. This difficulty can be explained by looking at the behavior of the singular values of  $\mathbf{A}_{js}$ . Fig.4 gives some examples for the singular values which resulted from the SVD of the  $\mathbf{A}_{js}$  matrix. In the case of the PWDM, as  $k$  become large, one observes that the singular values separate into two groups: rather than having one distinctly smaller singular value, we obtain a whole set of them. Accordingly, we can define a numerical ‘null space’ of the  $\mathbf{A}_{js}$  matrix. The interpretation of this null space is quite clear. It is well known [14, 15] that it is not efficient to include much more than  $N_{sc}$  plane-waves in the basis set  $F_j(x; k)$ , where

$$N_{sc} = \frac{1}{\pi} kL \quad (18)$$

and  $L$  is the perimeter of the billiard. The reason for this ineffectiveness is that  $k_i$  and  $k_j$  cannot be distinguished numerically within the interior region unless  $|k_i - k_j|L > 1$ . In order to obtain the semiclassical result (18), we divide the total phase space area ( $L \times (2mv)$ ) of the boundary Poincaré section by the size of Planck cell ( $2\pi\hbar$ ). If we use  $N > N_{sc}$  plane-waves, then we can create wavefunctions that are nearly zero in the interior, and become large only as we go far away from the center. Such superpositions are called ‘evanescent’ [16]. It is clear that the SVD can be used to determine the  $N - N_{sc}$  null space of evanescent states. Whenever  $k$  is an eigenvalue, this null space includes, in addition to the evanescent waves, the single eigenvector that constitutes an eigenstate of the Helmholtz equation. The problem is to distinguish this eigenvector from the other vectors in the null-space.

For the later numerical discussion of the PWDM, it is useful to characterize the numerics using

$$b = \frac{N}{N_{sc}} = \left|_{M=N} \frac{\lambda/2}{\Delta s} \right. \quad (19)$$

The latter equality holds if we take  $M = N$ , leading to the interpretation of  $b$  as the number of boundary points per half De-Broglie wavelength. If  $b < 1$  the null space problem does not exist, and we can define  $\mathbf{C}$  as the (left) eigenvector that corresponds to the smallest singular value of  $\mathbf{A}_{js}$ . Of course, we want to push PWDM to the limit, and therefore in practice we always take  $b > 1$ . One may naturally wonder whether choosing a very large  $b$  is numerically useful. Or, as a related issue, whether one gains anything from taking  $M > N$ . In the following section, it will become clear that taking  $b > 1$  does improve the numerics, while  $b \gg 1$  generally leads to instabilities that should be avoided. The optimal choice of  $b$  depends on the details of the implementation and on the computer hardware. It should be clear that if the numerical accuracy were unlimited, then the  $b \rightarrow \infty$  limit should lead to numerically exact solutions, though the convergence may be very very slow. This follows from the observation that plane-waves can serve as a complete basis: In principle any evanescent feature of the wavefunction can be reconstructed by a suitable superposition of plane-waves [16]. As for the the  $M > N$  issue, contrary to the impression that one may form from reading past literature, our experience (and see also [10]) has been that using  $M > N$  does not have a significant effect. Therefore, as a default we simply take  $M = N$ .

Finally, it should be noted that an effective way to get significant improvements with the DEM is to increase  $N$  by going beyond the PWDM. By adding different types of functions into the expansion, we can effectively increase  $N_{sc}$ . Specific ad-hoc recipes for this kind of improvement has been introduced in past literature (see eg [8]). In a follow-up paper [12] we integrate these and other recipes into the present unified framework.

### C. The metric method

The mathematically ‘clean’ solution for the null-space problem is to adopt a metric method. Unfortunately, as we explain in the next few paragraphs, this procedure is sensitive to cumulative numerical errors. What we are going to discuss is the straightforward version of the metric method. A modified implementation of the metric method, that avoids some of the numerical problems to be discussed below, had been introduced by Barnett [10].

In practical numerical implementations, the vector  $\mathbf{C}_j$  is normalized in the sense that  $\sum_j |\mathbf{C}_j|^2 = 1$ . Therefore,  $\Psi_r$  of Eq.(6) is not normalized appropriately within the interior region. By using the derivative of Eq.(17) in Eq.(11), and substituting into Eq.(14), we get the following numerical expression for the proper normalization factor:

$$\|\Psi_r\| = \Delta s \sum_s \mathbf{w}_s \left( \sum_j \mathbf{C}_j \mathbf{D}_{js} \right)^2 \quad (20)$$

$$= \sum_{ij} \mathbf{C}_i \mathbf{B}_{ij} \mathbf{C}_j = \mathbf{C} \mathbf{B} \mathbf{C}^\dagger \quad (21)$$

The definitions of  $D_{js}$  and of the metric  $B_{ij}$  can be found in Table 1. Following [7] the tension is defined as the boundary integral

$$\|\Psi_s\| = \Delta s \sum_s \left( \sum_j \mathbf{C}_j \mathbf{A}_{js} \right)^2 \quad (22)$$

$$= \sum_{ij} \mathbf{C}_i \mathbf{T}_{ij} \mathbf{C}_j = \mathbf{C} \mathbf{T} \mathbf{C}^\dagger \quad (23)$$

The standard practice to date for the tension calculation has been to use a denser set of boundary points located between the  $x_s$  points. However, our experience (see also [10]) is that the tension estimate obtained from the initial set of points is just as effective. This is demonstrated in Fig.3d. Therefore we routinely rely on the same set of boundary points to determine the tension.

The normalization  $\|\Psi_r\|$  and the tension  $\|\Psi_s\|$  can be calculated using the metrics  $\mathbf{B}_{ij}$  and  $\mathbf{T}_{ij}$  respectively. This method looks quite elegant, but it turns out not to be very effective numerically. Consider Eq.(20). This equation is quite safe computationally for two reasons: (i) all its terms are non-negative; (ii) standard summation routines order these terms in descending order. Now, let us look instead at Eq.(21). In this case the numerical calculation can give *any* result (if we go to large  $k$ ). Sometimes, the answer even comes out to be negative! This occurs because the calculation involves many arbitrarily ordered terms that each have a different algebraic sign.

The metric method works as follows: First, one finds the basis in which the normalization metric  $\mathbf{B}_{ij}$  becomes  $\delta_{ij}$ . The tension metric  $\mathbf{T}_{ij}$  should then be written in that same basis. The SVD is done on the transformed

tension metric. In this case, the null space becomes at most one-dimensional (whenever  $k = k_n$ ). Unfortunately, this elegant and straightforward metric scheme does not work very well, due to the finite precision problems discussed in connection with Eq.(21) and Eq.(23). Furthermore,  $\mathbf{B}$  and  $\mathbf{T}$  are ”squares” of  $\mathbf{A}$ , which leads to a loss of numerical precision compared with an  $\mathbf{A}$ -based strategy.

### D. Heller’s method

The most widely used  $\mathbf{A}$ -based strategy is referred to as Heller’s method [7]. The idea is to find  $\mathbf{C}_j$  as the solution of the  $M \geq N$  set of equations  $\sum_j \mathbf{C}_j \mathbf{A}_{js} = 0$ , with the additional constraint  $\sum_j \mathbf{C}_j \mathbf{A}_{j0} = 1$ . Table 1 gives the definition of  $\mathbf{A}_{j0}$ .

By constraining the wavefunction to be  $\Psi(X_0) = 1$  at a selected point  $X_0$  in the interior of the billiard, we eliminate the problems associated with evanescent states, so that we no longer have the null-space problem. As a result, quite large  $b$  can be used without encountering numerical instabilities. The only worry with this method is that  $X_0$  may happen to be very close to a nodal line. In such cases, the tension will be large due to improper normalization, so we will miss these eigenstates.

## IV. THE GFM AND DEM

In addition to providing a boundary method of its own, the GFM also serves to bridge the gap between the BIM and the DEM. Consider the version of the GFM that is based on the choice  $\mathcal{C}(x, x') = F_j(x; k)$ , where the  $F_j$  are solutions of the Helmholtz equation in free space (with neither singularities nor cuts). With this choice, we immediately realize that the DEM and the GFM are dual methods:

$$\mathbf{A} \Phi = 0 \quad [\text{GFM equation}] \quad (24)$$

$$\mathbf{C} \mathbf{A} = 0 \quad [\text{DEM equation}] \quad (25)$$

The only difference lies in whether one looks for the *left* or the *right* eigenvector. This point is numerically demonstrated in Fig.2.

The PWDM version of the DEM also satisfies this duality. In this special case, a somewhat more elegant version of the above argument is as follows: Consider the version of the GFM that is based on the choice  $\mathcal{C}(x, x') = \exp(ikn_j \cdot (x - x'))$ , where  $n_j$  is a unit vector in a given direction. We can take  $N$  different choices of  $n_j$ , thus obtaining the matrix equation  $\mathbf{A} \Phi = 0$  with

$$\mathbf{A}_{js} = \exp(ikn_j \cdot x_s) \quad (26)$$

An equivalent matrix equation is found by multiplying each equation by  $\exp(ik\phi_j)$ , where  $\phi_j$  are random phases. We can then take the real part of these equations, thus

obtaining a set of equations that involves the same matrix  $\mathbf{A}$  as that of PWDM, namely (5) with the basis defined by (2).

The duality of the PWDM and the GFM is very important from a mathematical point of view. The mathematical foundations of the PWDM are quite shaky. It is clear that PWDM is well-established mathematically if we have a so-called ‘inside-outside duality’ (IOD) [15]. Having an IOD in a strict sense implies that the boundary of the billiard may be regarded as a nodal line of some plane-wave superposition. Obviously, this is rarely the case [16]. Therefore, one may wonder whether we indeed have  $\det(\mathbf{A}) = 0$  whenever  $k = k_n$ . Using the duality Eq.(24), it is obvious that the Fredholm determinant is still a useful tool for quantization, even in the absence of an exact IOD.

It is quite clear from the first paragraph of this section that any expansion method can be associated with a corresponding GFM. Whenever the left eigenvector is used with the expansion method, the right eigenvector can be used with the GFM. We have already demonstrated this point in Fig.2. Is it possible to make the inverse statement? Do we have a well defined expansion method associated with any GFM? The answer is negative. We discuss this issue in the rest of this section, and it can be skipped at first reading.

For the following, it is convenient to consider Eq.(6) as  $N \rightarrow \infty$ . Subsequently, we are going to talk about whether this limit is meaningful. In the case of the usual PWDM, the  $N \rightarrow \infty$  limit of Eq.(6) can be written as

$$\Psi(x) = \int_0^{2\pi} C(\theta) d\theta \exp(ikn(\theta) \cdot x) \quad (27)$$

Similarly, in the case of the  $J_0$  decomposition, using the basis functions of Eq.(4), we can write in complete analogy:

$$\Psi(x) = \oint \Phi(s) ds J_0(k|x - x(s)|) \quad (28)$$

In writing Eq.(28) we have used the fact that  $J_0(x(j) - x(s))$  is a symmetric kernel, and therefore we could make the substitution  $\mathbf{C} = \Phi$ .

Eq.(28) looks at first sight like an innocent variation of Eq.(27). The Bessel function  $J_0$  is just a superposition of plane waves, and therefore one may possess the (incorrect) idea that there is a simple way to go from Eq.(28) to Eq.(27). If we expand each  $J_0$  in Eq.(28) in plane waves, and re-arrange the expression in order to identify the PWDM coefficients, we end up with the relation

$$\mathbf{C}(\theta) = \int e^{-ikn(\theta) \cdot x(s)} \Phi(s) ds \quad (29)$$

This relation implies the trivial result  $\mathbf{C}(\theta) = 0$  due to gauge freedom [see discussion of Eq.(26)]. Hence we conclude that the constructed wavefunction is  $\Psi(x) \equiv 0$  in the  $N \rightarrow \infty$  limit!

Having  $\Psi(x) \equiv 0$  from Eq.(28) could have been anticipated using a simpler argument: We know that Eq.(10) should hold for *any* gauge choice. This gauge freedom implies that we have

$$\oint \mathbf{C}(x, x(s)) \Phi(s) ds = 0 \quad (30)$$

The above equation should hold for any  $x$  inside as well as on the boundary. Furthermore, the left hand side of (30) is manifestly a solution of Helmholtz equation in free space, and it follows from the unique continuation property that Eq.(30) holds also for points outside of the boundary. Having  $\Psi(x) = 0$  as a result of the integration in Eq.(28) is just a particular case of Eq.(30).

In spite of the observation that Eq.(28) yields  $\Psi(x) \equiv 0$  in the  $N \rightarrow \infty$  limit, the vector  $\Psi_r$  is non-zero numerically for any finite  $N$ . In fact, after proper renormalization,  $\Psi_r$  becomes a quite good approximation to the wavefunction (see Fig.3c and Fig.3e). Sometimes the result so obtained is even better than the one which is found via the traditional BIM Eq. (7). As strange as it sounds, this success is entirely due to the fact that we are using finite  $N$ .

## V. THE QUANTIZATION MEASURE

Once we have constructed the wavefunction at a given  $k$ , the next step is to determine whether  $\Psi$  is an eigenstate. As we will explain below, our choice of measures reduces to finding the minima of one of:

$$S(k) = \text{tension} \quad (31)$$

$$S(k) = \text{smallest singular value} \quad (32)$$

$$S(k) = \text{determinant} \quad (33)$$

Here, ‘determinant’ is used to represent the product of all the singular values. Two questions arise: (i) Are these measures mathematically equivalent? (ii) Are they numerically equivalent? The first of these questions is easily resolved, while the second one requires a somewhat more lengthy discussion.

We first settle the simpler question of the mathematical equivalence. The BIM Eq. (12) and the GFM Eq. (13) can both be written as  $\mathbf{A}\Phi = 0$ , with the appropriate choice of  $\mathbf{A}$ . Thus, if  $k$  is an eigenvalue,  $\mathbf{A}$  must have a singular value that tends to 0 as  $N$  is increased. The determinant is just the product of all the singular values, and therefore it vanishes whenever one of the singular values does. At the same time, the constructed wavefunction should have small tension. It follows that low tension must be correlated with having vanishingly small singular value. Thus in the large  $N$  limit all three quantization measures are mathematically equivalent.

The argumentation above implies that neither the traditional implementation of PWDM, nor that of the BIM should be considered to be ‘package deals’. For example, the BIM could be used with the tension as a measure,

rather than looking for minima of the the singular values. Similarly, the usual Heller method for the PWDM could be replaced by a search over determinant values.

### A. The tension as a quantization measure

The tension is a robust measure for quantization. Fig.5 displays some examples of the corresponding  $S(k)$  plots. The PWDM minima are typically much ‘sharper’ than their BIM equivalents. Zooming over a PWDM minimum (Fig.5d) reveals some amount of roughness. This feature is actually helpful, because it gives an indication of and control over the stability of the numerics. We interpret the roughness of the PWDM minimum as a reflection for the existence of a null-space. In the same spirit, the smoothness of the BIM minima can be regarded as an indication that better accuracy can be obtained by making  $N$  larger. We discuss this issue further below.

The tension provides a common measure that may be used to monitor improvements, as well as to compare the success of the different methods. Naturally, the first issue to discuss is the dependence of the tension on the size  $N$  of the basis set (see Fig.6). For the BIM, the tension becomes better as  $N$  grows, and disregarding the computer hardware, there is no reason to suspect that there is an inherent limitation on the accuracy. The situation is different for the PWDM. Here, taking  $N$  much larger than  $N_{sc}$  is not effective. In practice, the method reaches a limiting accuracy, which, taking into account present hardware limitations, is still very good compared with that of the BIM.

From Fig.6, it is also clear that the tension of the PWDM becomes much better as  $k$  becomes larger. This is expected on the basis of the following semiclassical reasoning: larger uncertainties in  $k$  result from confining a particle to a smaller box (taking a smaller box for a given  $k$  is equivalent to making  $k$  smaller for a given box size). Thus, it is more difficult to build a wavefunction with a precise value of  $|k_j| = k$  for low lying eigenstates. On the other hand, the BIM does not seem to be sensitive to the value of  $k$ .

The tension can be regarded as a measure of the *local error* in the determination of the eigenfunction. The tension is ‘local’ in the sense that it pertains only to points along boundary. We can also define a measure for the *global error*: That is the error which is associated with all the interior points.

$$(\Delta\Psi)^2 = \langle |\Psi_r - \Psi_{\text{exact}}(X_r)|^2 \rangle \quad (34)$$

Here  $\Psi_{\text{exact}}(x)$  is the numerically exact wavefunction. The average is taken over the set  $X_r$  of selected points inside of the boundary. Fig.7 gives an example for the variation of the error along the cross section line of Fig.1. In order to eliminate a possible bias due to a global normalization-error, we re-normalized the ‘non-exact’ wavefunction so that  $\Psi_r = \Psi_{\text{exact}}(X_r)$  at the selected point  $X = X_0$ . In

retrospect, we realized that such an error did not significantly affect the result. However, we still chose to be on the safe side, and we adopted this procedure routinely.

It is natural to expect the average error  $(\Delta\Psi)^2$  to be correlated with the tension. In other words, if  $|\Psi_r - \Psi_{\text{exact}}(X_r)|$  is small on the boundary, then one may expect it to be small in the interior. The degree of such correlation is important for practical reasons. Moreover, we have introduced two different versions of tension definitions, one for each of the PWDM and the BIM. It is not a-priori clear that the above correlation is independent of the choice of numerical method. In Fig.8, we study this issue by plotting  $(\Delta\Psi)^2$  against the tension for the BIM and the PWDM. In the case of the PWDM, the error saturates below a critical tension. Below this point, further improvements on the boundary do not seem to affect the bulk of the eigenstate. It is not clear from the numerics that the BIM show this saturation. In any case we see that for the same tension, the BIM does a poorer job in reproducing the wavefunction inside of the boundary.

The saturation of the error well inside the billiard can be explained as a manifestation of the fact that the wavefunction there is not very sensitive to sub-wavelength roughness of the boundary: If  $N$  is reasonably large, the numerical wavefunction vanishes on a nodal line that almost coincides with the true (pre-defined) boundary. Increasing  $N$  further affects the sub-wavelength features of the (distance) difference between that nodal-line and the true boundary. This distance difference is important for the tension, but not very it is not very important for the wavefunction well inside the billiard.

### B. The determinant as a quantization measure

As we have already discussed in the introduction, the tension is the natural measure of quantization. However, from a numerical point of view, it is much more convenient and time efficient to compute the singular values of  $\mathbf{A}$ , without having to find the eigenvectors for each  $k$  value, and without having to compute the wavefunction along the boundary (for tension calculation).

The smallest singular value is traditionally used as a quantization measure for the BIM. From Fig.7, it is quite clear that one of the singular values is significantly smaller than the others, so that the eigenstate is unambiguously determined by this method. Is it possible to use the same approach, with comparable success, for the PWDM? We have already determined that looking at the smallest singular values is not very meaningful numerically. For  $N > N_{sc}$ , there exists a large null-space of evanescent states for any  $k$ , unless we use a metric method. However, the metric method is numerically complicated, so let us not take it as a practical option. Can we do better? Each time that  $k = k_n$ , the null space should include one more ‘dimension’. Therefore, the determinant, rather than the smallest singular value, becomes the reasonable quantity to look at. Thus, from

numerical point of view, (32) should be superior to (31).

Fig.9 illustrates how the determinant can be used in practice as a quantization measure. As a general rule, as is the case for the tension, the PWDM/GFM minima are ‘sharper’ than the BIM ones. On the one hand, this extra sharpness can be regarded as an advantage, because it leads to a better resolution of the eigenvalue spectrum. However, more computer time is needed in order to find these minima. The BIM minima are broader, and therefore ‘digging’ algorithms that search for local minima become extremely effective.

In the case of the traditional BIM, using a larger  $N$  leads to a better resolution of the local minima, as expected. The traditional H-BIM uses the complex Hankel Bessel function as its Green function. One may wonder why the real Neumann function could not be used instead. A-priori, there is no reason to insist on Hankel choice. However, it seems that with Neumann choice the numerics are not very stable: The locations of the local minima vary on a  $k$  range which is large compared to their  $k$  width. Because of this problem, search routines in case of Y-BIM may yield misleading values for the error in the  $k_n$  determination. The numerical stability of the H-BIM can be attributed to the fact that the BIM equation  $\mathbf{A}\Phi = 0$  becomes complex. Its real part is just the Y-BIM equation, while its imaginary part is the J-GFM equation. Thus one may say that the H-BIM benefits from combining the Y-BIM with the J-GFM.

Is it always possible to use the Fredholm determinant as a quantization measure in the GFM/PWDM case? Here we observe that the null-space problem is reflected in the stability of the determinant calculation. For  $1 < b < 1.8$ , we get nice minima, which actually look much sharper than the BIM ones. However, we are faced once again with the usual problem: As we try to increase  $b$  in order to improve accuracy, the numerics loose stability. This is illustrated in Fig.10 for the PWDM case. The same phenomenon occurs with J0-GFM, which has somewhat larger tendency for instability. This is apparently because the J0-GFM is involved with a larger null-space (see Fig.4). The larger null-space in the case of the J0-GFM is probably related to the fact that the  $J_0$  basis functions are quite localized on the boundary, so that as a result they span a smaller space of non-evanescent wavefunctions. Note also our discussion in Sec.III-C.

## APPENDIX A: THE BIM FOR THE SCATTERING PROBLEM

The solution of the Helmholtz equation for the scattering problem is just another variation of the BIM. Consider a boundary, one that in general may be composed of several disconnected pieces. The incident wave  $\Psi_{\text{incident}}(x)$  is a solution of Helmholtz equation in free space. Formally,  $\Psi_{\text{incident}}(x)$  includes both the ingoing and the outgoing wave components. We look for a solution  $\Psi(x)$  that has the same ingoing component as

$\Psi_{\text{incident}}(x)$ , and that satisfies  $\Psi(x) = 0$  on the boundary. Such solution can be written as a sum of the incident wave and a scattered wave, and hence must be of the form

$$\Psi(x) = \Psi_{\text{incident}}(x) + \oint G(x, x(s'))\Phi(s')ds' \quad (\text{A1})$$

Equation (A1) is a variation of Eq.(10). Note that the Green function should satisfy outgoing boundary conditions in order to yield the desired solution. The charge density  $\Phi(s)$  is fixed by the requirement that  $\Psi(x) = 0$ , which leads to the boundary equation

$$\oint G(x(s), x(s'))\Phi(s')ds = -\Psi_{\text{incident}}(s) \quad (\text{A2})$$

This inhomogeneous equation is a straightforward generalization of Eq.(12). A discretized version of it was used in Ref.[17] in order to obtain numerical solutions of the Helmholtz equation for some scattering problems.

The derivation of Eq.(A2) in Ref.[17] is much more complicated than ours, and involves the use of Lippmann-Schwinger equation. The boundary is represented by a large delta-potential  $V$ , and the limit  $V \rightarrow \infty$  is taken. Using this procedure, the charge density  $\Phi(s)$  can be obtained as the  $V \rightarrow \infty$  limit of  $V\Psi(x(s))$ . Note the correctness of the physical units. Namely,  $[\mathcal{H}][\Psi] = [\rho]$  and therefore  $[V][\Psi] = [\Phi]$ . Note also that the wavefunction is in general non-zero in both sides of the boundary. Therefore the charge density  $\Phi(s)$  is equal to the *difference* between the normal derivatives on both sides of the boundary. The simplest way to derive the relation between  $\Phi(s)$  and  $V\Psi(x(s))$  is to integrate the Helmholtz equation over an infinitesimal range across the boundary, as in the treatment of the 1D Shchrodinger equation with delta potential.

## APPENDIX B: TRADITIONAL BIM

The primitive BIM equation (Eq.(12)) is based on Eq.(10). The traditional BIM is a variation of the same idea. Rather than using Eq.(10) directly, one considers its gradient, leading to

$$\partial_{\pm}\Psi(x(s)) = \oint \partial_{\pm}G(x(s), x(s'))\Phi(s')ds' \quad (\text{B1})$$

This equation is analogous to Eq.(12). We use the notation  $\partial_+$  and  $\partial_-$  in order to refer to the normal derivative on the interior and exterior sides of the boundary respectively. By definition,  $\partial_- \Psi(x(s)) = \Phi(s)$ , and from the discussion in section III we have  $\partial_+ \Psi(x(s)) = 0$ . Adding the two equations of (B1), we obtain

$$\Phi(x(s)) = \oint 2\partial G(x(s), x(s'))\Phi(s')ds' \quad (\text{B2})$$

where  $\partial \equiv (\partial_+ + \partial_-)/2$  is just the derivative on the boundary in the principal sense. Thus, in the traditional

BIM, the definition of the Fredholm matrix is

$$\mathbf{A}_{ss'} = \frac{1}{\Delta s} \delta_{ss'} - 2\partial G(x(s), x(s')) \quad (\text{B3})$$

and the BIM equation (B2) is  $\mathbf{A}\Phi = 0$ . The kernel  $\partial G(x(s), x(s'))$  is well behaved, and its diagonal elements are finite thanks to the presence of a geometrical factor. Namely, if  $G(x(s), x(s')) = g(k|x(s) - x(s')|)$  then

$$\partial G = k \frac{n(s) \cdot (x(s) - x(s'))}{|x(s) - x(s')|} g'(k|x(s) - x(s')|) \quad (\text{B4})$$

If either one of the Bessel functions  $H_0$  or  $Y_0$  is used for the Green function, then the definition of  $\mathbf{A}_{ss'}$  above

involves either  $H_1$  or  $Y_1$ , respectively.

#### Acknowledgments:

It is our pleasure to thank Alex Barnett, Areez Mody, Lev Kaplan and Michael Haggerty for many useful discussions. This work was funded by ITAMP and the National Science Foundation.

- 
- [1] H.J. Stockmann, "Quantum Chaos : An Introduction" (Cambridge Univ Pr 1999).
  - [2] S. Datta, "Electronic Transport in Mesoscopic Systems" (Cambridge Univ Pr 1997).
  - [3] E.J. Heller, Phys. Rev. Lett. **53**, 1515 (1984).
  - [4] M. Robnik, J. Phys. A **17**, 1049 (1983).
  - [5] G.A. Luna-Acosta, Kyungsun Na, and L.E. Reichl, Phys. Rev. E **53**, 3271 (1996).
  - [6] M.V. Berry and M. Wilkinson, Proc. R. Soc. London A **392**, 15 (1984).
  - [7] E.J Heller, *Chaos and Quantum Systems*, ed. M.-J. Giamanni, A. Voros, J. Zinn-Justin (Elsevier, Amsterdam, 1991), p. 548.
  - [8] E. Vergini, PhD thesis (Universidad de Buenos Aires, 1995).
  - [9] E. Vergini and M. Saraceno, Phys. Rev. E, **52**, 2204 (1995).
  - [10] A. Barnett, PhD thesis (Harvard, Sept. 2000).
  - [11] B. Li, M. Robnik, B. Hu, Phys. Rev. E **57**, 4095 (1998).
  - [12] N. Lepore, D. Cohen and E.J. Heller, in preparation.
  - [13] P.A. Boasman, Nonlinearity **7**, 485.
  - [14] B. Dietz and U. Smilansky, Chaos **3**, 581 (1993).
  - [15] B. Dietz et al., Phys. Rev. E **51**, 4222 (1995).
  - [16] M.V. Berry, J. Phys. A, **27**, L391 (1994).
  - [17] M.G.E. da Luz, A. Lupu Sax, and E.J. Heller, Phys. Rev. E **56**, 2496 (1997).
  - [18] The polar equation of the Pond shape is  $r = 1 + 0.2 * \cos(\theta + 0.9 * \cos(\theta))$ .

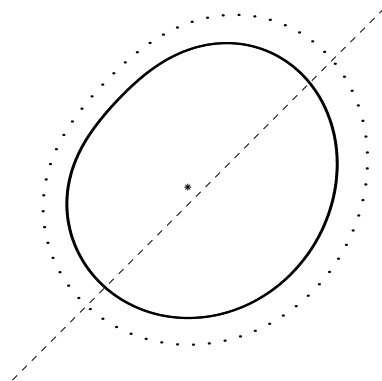


FIG.1: Full line: The 'Pond' shape [18]. Its radius is roughly 1, and its perimeter is  $L = 6.364$ . Dashed line: The cross section line that is used e.g. in Fig.3c. Dots: The 'outer boundary' which is used for the BIM tension calculation (see Sec.III-A). The transverse distance between the actual boundary and the outer boundary was chosen in most cases to be  $\Delta L \sim 10\Delta s$ . Star: The selected point which is used in Heller's implementation of the PWDM method.

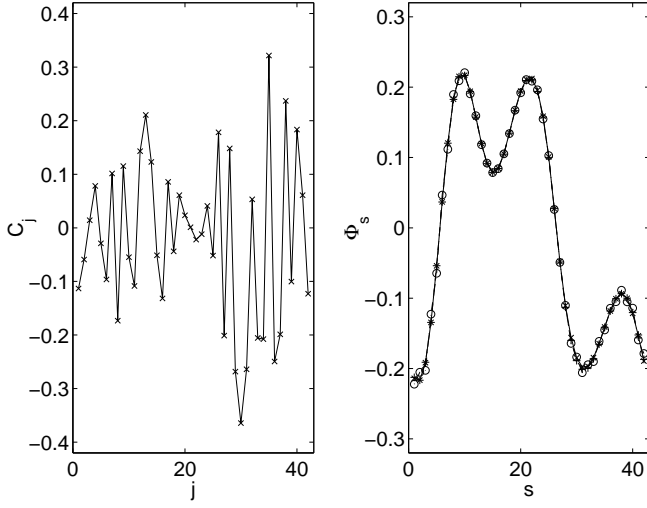


FIG.2: The eigenvectors of the Fredholm matrix (Eq.(5)) are found for  $k = k_n = 6.82754592867694$ . Right plot: The right-eigenvector  $\Phi$ . The symbols (x) and (+) and (o) correspond respectively to the PWDM choice of Eq.(2), to the H1-BIM choice of Eq.(B3), and to the J0-GFM choice of Eq.(4). Left plot: The left-eigenvector  $C$  for the PWDM Fredholm matrix. In the two other cases (H1-BIM, J0-GFM) the Fredholm matrix is symmetric and  $C = \Phi$ .

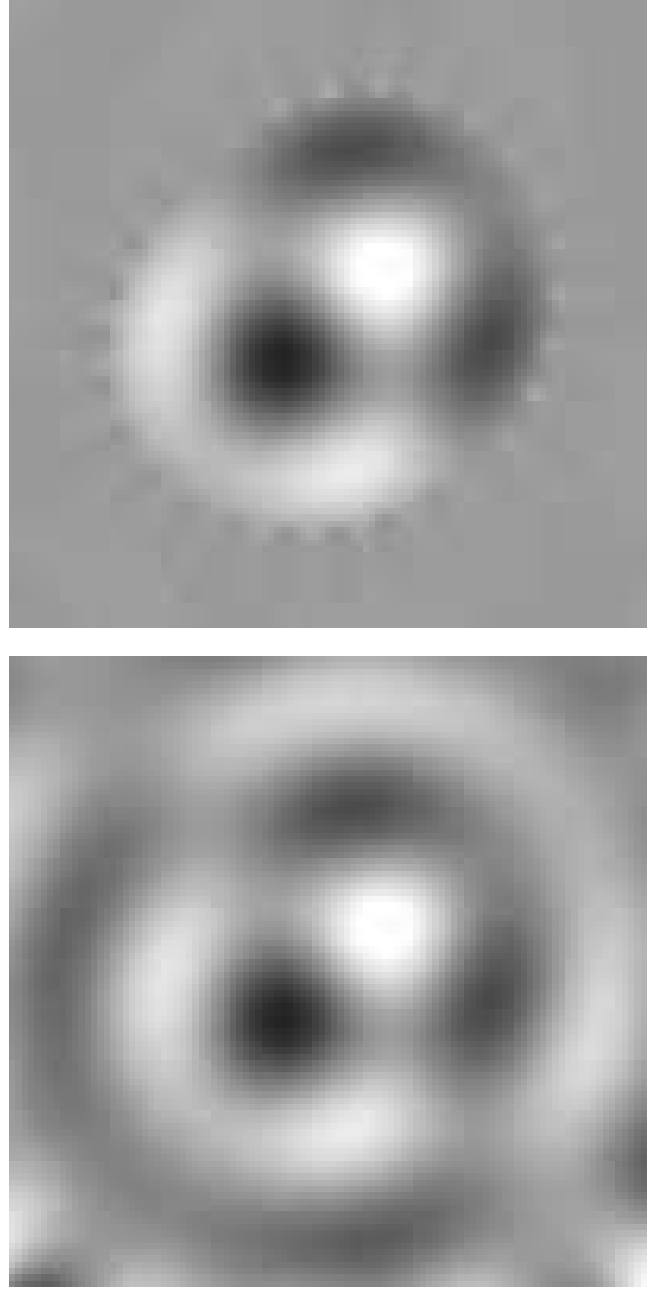


FIG.3: See the other panels and the caption in the next column.

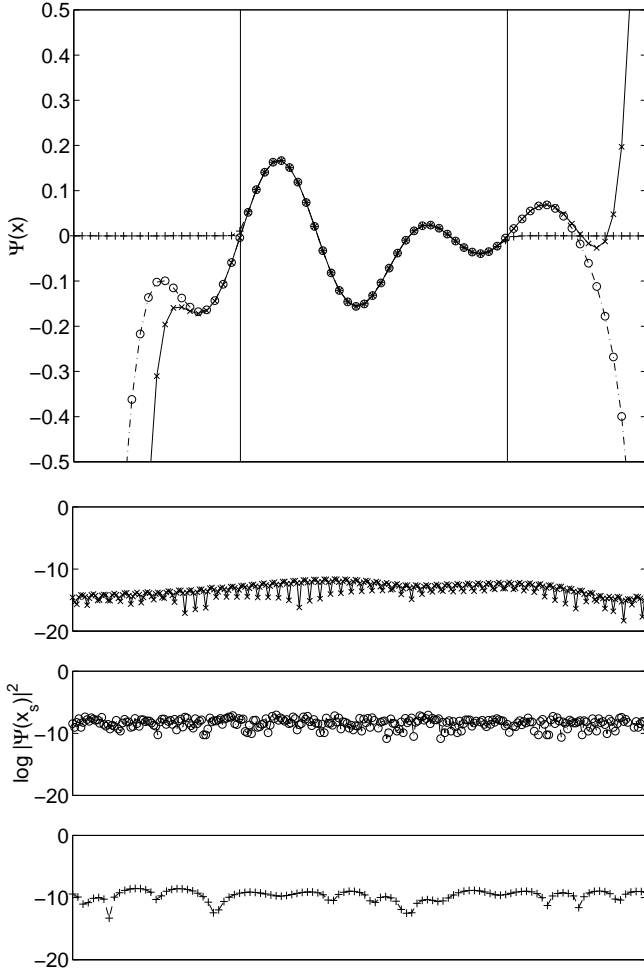


FIG.3: The eigenfunction at  $k = k_n$  is found using the eigenvectors of Fig.2. (a) An image of  $\Psi(x)$  using Eq.(7). (b) The same using PWDm and Eq.(6). (c) Plot of  $\Psi(x)$  along the crosssection line of Fig.1. The vertical lines indicate the location of the boundary. The wavefunctions that correspond to images a-b are shown with (+) and (x) respectively. We also show with (o) the wavefunction that is obtained using J0-GFM and Eq.(6). Panels d-e-f display plots of  $\log(|\Psi(x)|^2)$  along the boundary. The symbols are as in c.

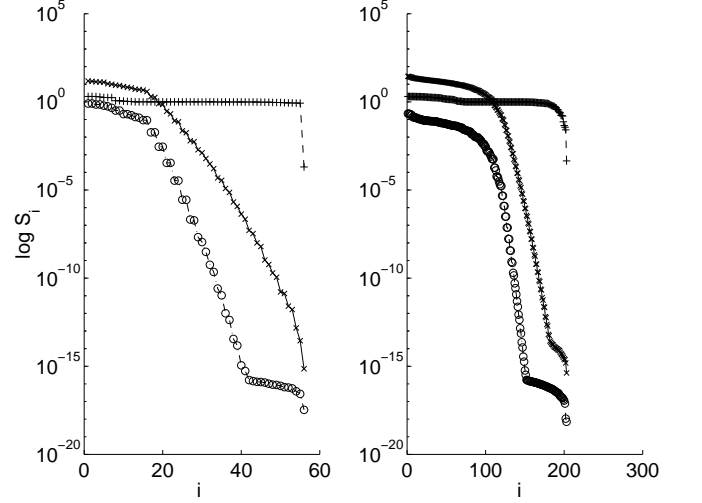


FIG.4: Singular values of the Fredholm matrix for  $k_n = 6.82754592867694$  (left panel) and for  $k_n = 50.05474912004408$  (right panel). The various symbols are as in Fig.2.

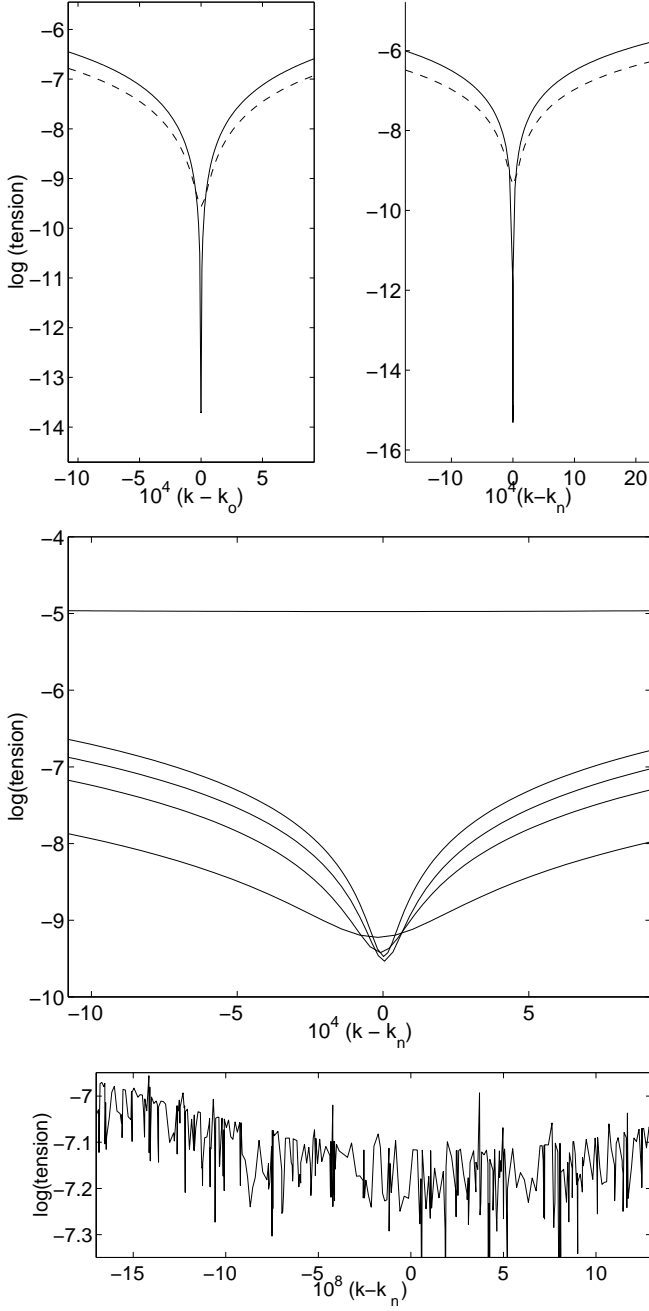


FIG.5: The tension as a function of  $k$  in the vicinity of  $k_n = 10.14707971517264$  (upper-left and lower panels), and of  $k_n = 50.05474912004408$  (upper right panel). In the upper panels (a-b) the full line is for the PWDm constructed wavefunction, while the dashed line is for the BIM constructed wavefunction. For the low  $k$  state we chose  $b = 4$ , while for the high  $k$  we used  $b = 2$ . Panel (c) demonstrates the dependence of the BIM tension on the choice of the distance  $\Delta L$ . The different curves (from the upper to lower) correspond to  $\Delta L/\Delta s = 1, 8, 16, 12, 4$ . Panel (d) is a zoom over the PWDm minimum.

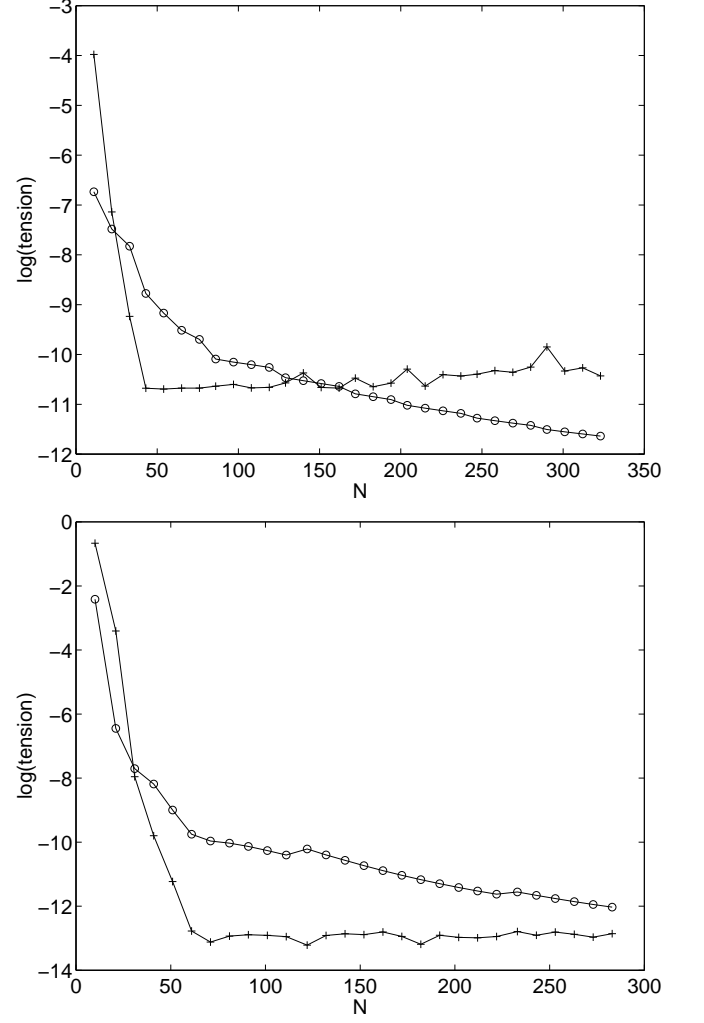


FIG.6: The tension for the constructed eigenstate versus the number  $N$  of basis functions. The upper panel is for the  $k_n = 2.40425657792391$  eigenstate, and the lower panel is for the  $k_n = 6.82754592867694$  eigenstate. The symbols (o) and (+) are for the BIM and for the PWDm, respectively.

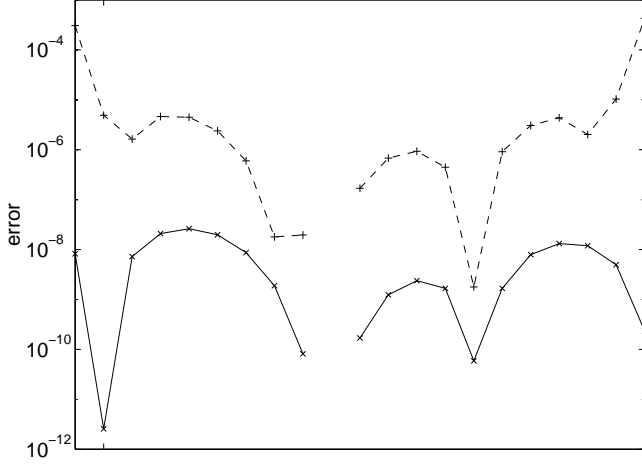


FIG.7: Plot of the error  $|\Psi_r - \Psi_{exact}(X_r)|^2$ , along the cross-section line of Fig.1. We refer here to the  $k_n = 6.82754592867694$  eigenfunction. The numerically ‘exact’ wavefunction is our best PWDM-constructed wavefunction ( $N = 69$ ) with tension  $= 10^{-13}$ . The ‘non-exact’ wavefunction is either BIM-constructed (+) or PWDM-constructed (x), with tension  $\approx 10^{-8}$ . In the middle point the error is zero by construction (see explanation in the text).

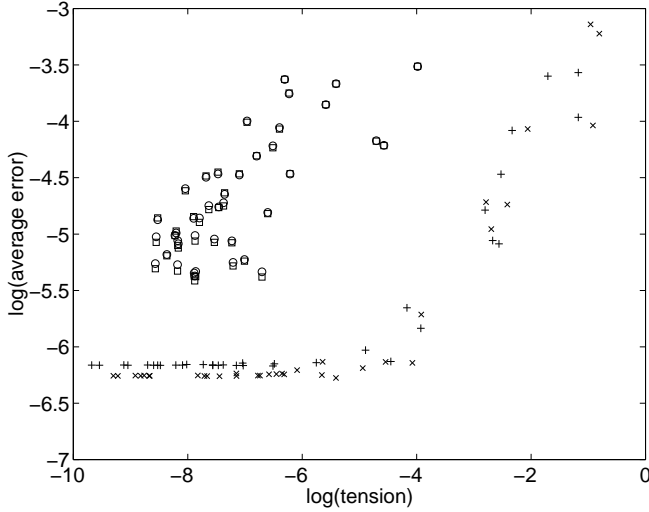


FIG.8: The averaged error in the determination of the wavefunction, versus the tension for the  $k_n = 6.82754592867694$  eigenfunction. For the BIM-constructed wavefunction we use squares and (o), while for the PWDM one we use (+) and (x). The error has been determined with respect to the ‘exact’ wavefunction  $\Psi_{exact}$ . The latter is numerically defined as either the best BIM eigenstate (squares and (+)) or as the best PWDM one ((o) and (x)). For both choices  $\Psi_{exact}$  had a tension better than  $10^{-10}$ .

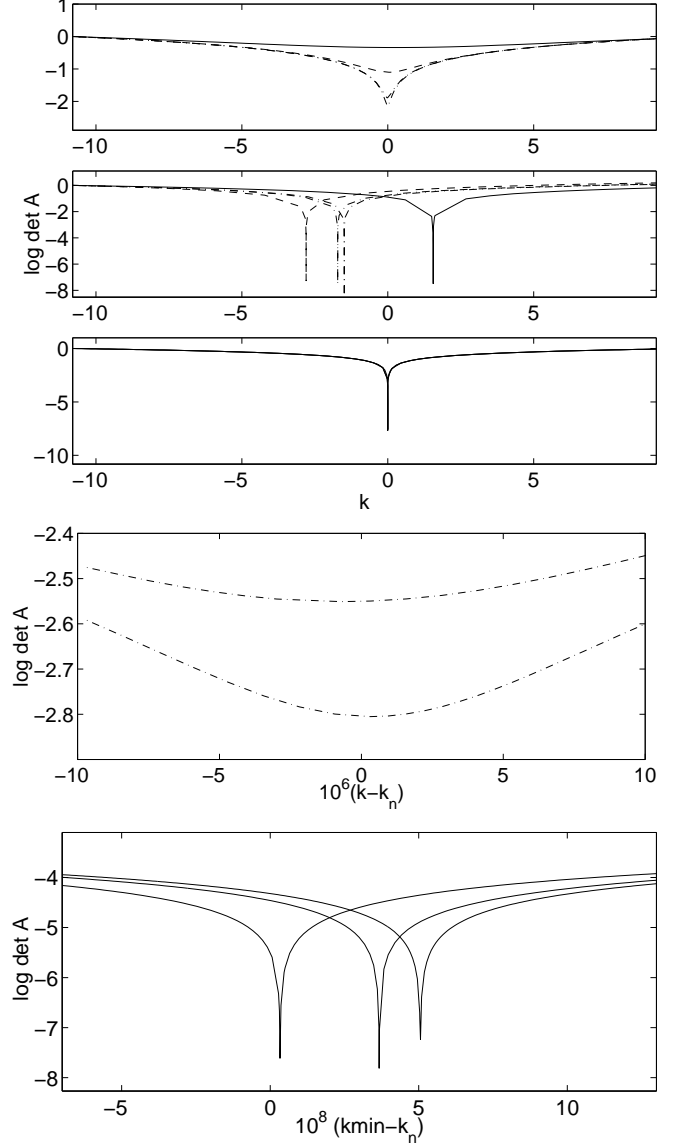


FIG.9: The Fredholm determinant ( $S(k)$ ) versus  $k$  in the vicinity of  $k_n = 10.14707971517264$ . Note that  $S(k)$  is normalized such that  $S(k) = 1$  away from the minima. Panels a-b-c show  $S(k)$  in the cases of the H1-BIM, the Y1-BIM and the PWDM, respectively. The lines plotted, in order of decreasing  $S(k)$  minimum, correspond to  $b = 2, 3, 4, 8$  in panel (a),  $b = 4, 8, 13, 12$  in panel (b) and  $b = 2$  in panel (c). Panels (d) and (e) give a zoom over the minima of panels (a) and (c), respectively. We witness some numerical instabilities for both the Y1-BIM and the PWDM, though in the latter case it is much much weaker, and can be resolved only in the zoomed plot (panel (e)). For larger  $b$  values, the PWDM instability is enhanced, and the results are reduced to numerical garbage (not shown).